JPE 16-2-39

http://dx.doi.org/10.6113/JPE.2016.16.2.805
ISSN(Print): 1598-2092 / ISSN(Online): 2093-4718

A Shared Channel Design for the Power and Signal Transfers of Electric-field Coupled Power Transfer Systems

Yu-Gang Su[†,*], Wei Zhou[*], Aiguo Patrick Hu[**], Chun-Sen Tang[*], and Rong Hua[**]

[†]State Key Laboratory of Power Transmission Equipment and System Security and New Technology, Chongqing University, Chongqing, China
[*]College of Automation, Chongqing University, Chongqing, China
[**]Department of Electrical and Computer Engineering, University of Auckland, Auckland, New Zealand

Abstract

Electric-field coupled power transfer (ECPT) systems have been proposed as an alternative wireless power transfer (WPT) technology in recent years. With the use of capacitive plates as a coupling structure, ECPT systems have many advantages such as design flexibility, reduced volume of the coupling structure and metal penetration ability. In addition, wireless communications are effective solutions to improve the safety and controllability of ECPT systems. This paper proposes a power and signal shared channel for electric-field coupled power transfer systems. The shared channel includes two similar electrical circuits with a band pass filter and a signal detection resistor in each. This is designed based on the traditional current-fed push-pull topology. An analysis of the mutual interference between the power and signal transmission, the channel power and signal attenuations, and the dynamic characteristic of the signal channel are conducted to determine the values for the electrical components of the proposed shared channel. Experimental results show that the designed channel can transfer over 100W of output power and data with a data rate from 300bps to 120 kbps.

Key words: ECPT, Electric-field coupled, Half-duplex communication, Shared channel, Wireless power transfer

I. INTRODUCTION

Wireless power transfer (WPT) technologies provide solutions for power transfer when direct wire connections are impossible or hard to achieve [1], [2]. Electric-field Coupled Power Transfer (ECPT) is a wireless power transfer technology that has been used in rotating devices [3], mobile robots [4], biological implants [5], cell phones [6], and electric vehicles [7], [8]. With the use of capacitive plates as coupling structures, ECPT has many advantages such as design flexibilities, a small volume of the coupling structure and metal penetration capability [9], [10]. Fig. 1 shows a block diagram of a typical ECPT system.

Manuscript received Jun. 29, 2015; accepted Oct. 10, 2015
Recommended for publication by Associate Editor Jee-Hoon Jung.
[†]Corresponding Author: su7558@qq.com
Tel: +86-23- 65112750, Fax: +86-23- 65111221, Chongqing University
[*]College of Automation, Chongqing University, China
[**]Dept. of Electrical and Computer Eng., University of New Zealand, New Zealand

For ECPT systems, a challenge is to achieve large amounts of output power and high power transfer efficiency [11]-[15]. The signal communication system between the transmitter and the receiver can help achieve a high output power and efficiency.

Many wireless signal transfer strategies have been proposed for inductively coupled power transfer (ICPT) systems. A signal channel whose frequency is closed to the power transfer frequency using two auxiliary coils has been prsented [16], [17]. A power and signal transfer method was proposed for mini equipment with an operating frequency greater than 1MHz and a 12mW transfer power [18], [19]. Additionally, a high-speed and accurate controller is used to modulate a signal for avoiding noise due to the current switching in an inverter, which aids in the simultaneous transfer of power and signals [20]. However, due to essential differences between ECPT and ICPT systems, the power and signal transfer methods for ICPT systems cannot be directly applied to ECPT systems. Therefore, this paper proposes a

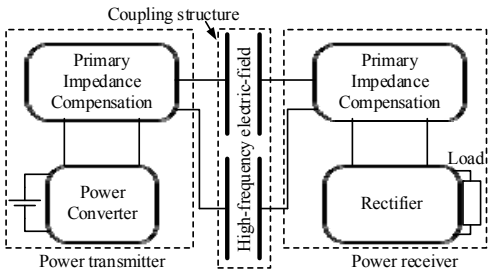

Fig. 1. Block diagram of a simplified ECPT system.

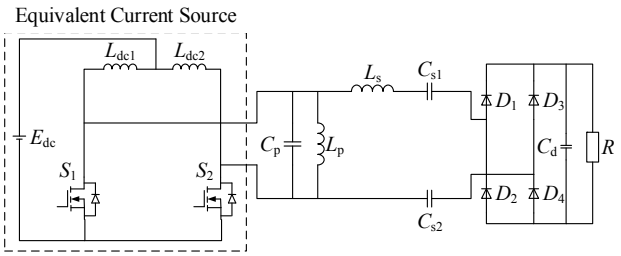

Fig. 2. Traditional current-fed push-pull topology of ECPT system.

power and signal shared channel for ECPT systems.

Section II, introduces the shared channel structure and its operation principle based on a traditional current-fed push-pull method. The designed circuits are analysed using both dynamic and static analyses in Sections III and IV. Finally, simulations and experiments are conducted to evaluate the designed channel performance in Sections V and VI.

II. Topology for Power and Signal Parallel Transmission

A. Traditional ECPT Topology

A traditional topology of an ECPT system includes a current-fed push-pull resonant converter, a resonant tank, two electric plates and a voltage rectifier, as shown in Fig. 2. In this topology, a dc voltage E_{dc} is transformed into a quasi current by two phase-splitting inductors. The MOSFET drain voltage increases when the current go into the resonant tank. Due to manufacturer imperfections, one of the MOSFET will turn on when the other is off, and the tank circuit starts to resonate to generate an ac electric field. Two pairs of metal plates on the coupling structures can be modelled as the equivalent capacitors C_{s1} and C_{s2} (in Fig. 2). To transfer power to the load efficiently, the series coupling capacitors are tuned by the compensation inductor L_s at the operating frequency. The rectifier bridge D_1-D_4 inverts the AC voltage into a DC voltage to supply the load R directly.

B. Communication Signal Channel Design

The communication signal channel includes two coupling capacitors C_{s1} and C_{s2}, two branch circuits with two selective LC filters, and resistors that are built for conducting communication between the transmitting side and the receiving side. Fig. 3 shows the communication channel within the traditional ECPT system.

For wireless signal transmission, the combination of quasi-current source and push-pull inverter services is an AC current source which is equivalent to an open circuit for the signal channel. Therefore, the circuit before the parallel resonance tank is removed, as shown in Fig. 3, according to the simplification. In addition, the rectifier D_1-D_4, the filtering capacitor C_d, and the load R are together considered as a resistor load which is equal to R_L. In this signal channel, the capacitor C_b serves as an isolation capacitor which isolates the low-frequency power wave transfer across the communication branch circuits. To effectively keep the power wave out of the signal channel, the capacitor C_b has to be set as a small value.

A compensation inductor L_b is connected in series with the capacitor to select signals at a signal carrier frequency ω_s which can be calculated using Equation (1).

$$\omega_s = \frac{1}{\sqrt{L_b C_b}} \tag{1}$$

L_b has a negligible influence on the isolation characteristic of C_b because the tuning frequency of C_b and L_b, is equal to the signal carrier wave frequency which is much higher than the power transfer frequency. The signal carrier wave is modulated by the amplitude shift keying (ASK) mode which provides a small changing of the amplitude of the carrier wave during 0-1 shifting. The resistors R_{b1} and R_{b2}, which connect with the

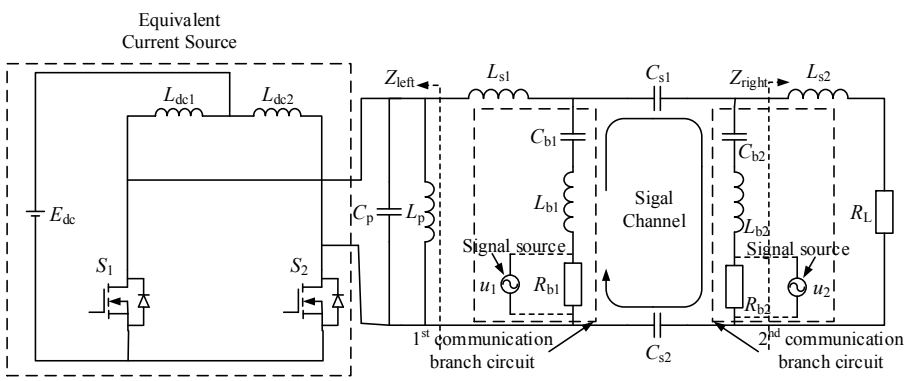

Fig. 3. Improved topology of ECPT system with communication branch circuit.

signal source can enhance the damping coefficient of the signal channel, and decrease the dynamic response time of the saltus step of the amplitude of the carrier wave which is detailed in a later section. During the half-duplex communicate operation, only one source is connected with R_{b1} (or R_{b2}), and another resistor R_{b2} (or R_{b1}) on the opposite side serves as signal detection resistor. Moreover, the compensation inductor L_s is divided into two inductors L_{s1} and L_{s2} to enhance the impedance of the branch circuit beside the signal branch circuit, which can increase the communication quality.

III. Steady State Analysis of Power and Signal Transmission

For wireless power and signal transfer systems, the quality of the systems are measured based on the levels of the interferences between the power transmissions and the signal transmissions.

A. Power Transmission

Fig.4 shows a simplified circuit of the power channel in which the current-fed push-pull inverter is considered as an AC current source.

If C_p and L_p are fully tuned to the system operating frequency, the AC output voltage of the push-pull inverter can be boosted by π times the input dc voltage, which is shown in Equation (2).

$$u_p = \pi E_{dc} \tag{2}$$

In Fig. 4, the voltage achieved by the load u_{RL} should be equal to the voltage on the parallel resonant tank u_p at the resonant frequency without considering the resistances of the internal components. The transfer function G_{RL} is presented in Equation (3).

$$G_{RL} = \frac{u_{RL}}{u_p} = 1 \tag{3}$$

Considering the impact of the signal on the power transfer and the impact of the power on the signal detection, the circuit in Fig. 4 is divided into four parts and the impedance of each part can be expressed as:

$$\begin{cases} Z_b = j\omega_p L_b + \dfrac{1}{j\omega_p C_b} + R_b \\ Z_{p1} = j\omega_p L_{s2} + R_L \\ Z_{p2} = \dfrac{1}{j\omega_p C_s} + \dfrac{Z_b Z_{p1}}{Z_b + Z_{p1}} \\ Z_{p3} = j\omega_p L_{s1} + \dfrac{Z_b Z_{p2}}{Z_b + Z_{p2}} \end{cases} \tag{4}$$

Where Z_{p1}, Z_{p2}, and Z_{p3} are the local impedances shown in the Fig.4. Z_b donates the impedance of the communication branch circuit and C_s=$C_{s1}C_{s2}$/(C_{s1}+$_{s2}$), L_b=L_{b1}=L_{b2}, C_b=C_{b1}=C_{b2}, and R_b=R_{b1}=R_{b2}. According to the Kirchhoff voltage and current laws (KVL and KCL), the intermediate transfer functions can be expressed as:

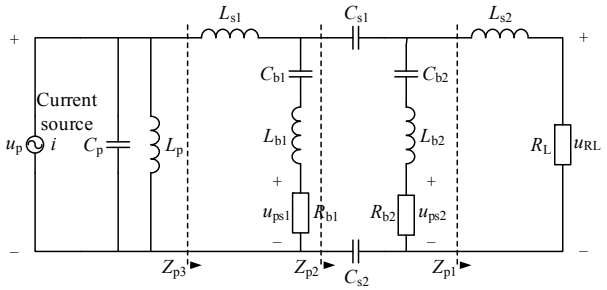

Fig. 4. Simplified circuit of power channel.

$$\begin{cases} G_{ad1} = \dfrac{i_{Ls1}}{u_p} = \dfrac{1}{Z_{p3}} \\ G_{ad2} = \dfrac{u_{b1}}{i_{Ls1}} = Z_{p3} - j\omega_p L_{s1} \\ G_{ad3} = \dfrac{u_{b2}}{u_{b1}} = \dfrac{j\omega_p C_s Z_{p2} - 1}{j\omega_p C_s Z_{p2}} \end{cases}, \begin{cases} G_{ad4} = \dfrac{u_{ps1}}{u_{b1}} = \dfrac{R_{b1}}{Z_b} \\ G_{ad5} = \dfrac{u_{ps2}}{u_{b2}} = \dfrac{R_{b2}}{Z_b} \\ G_{ad6} = \dfrac{u_{RL}}{u_{b2}} = \dfrac{R_L}{Z_{p1}} \end{cases} \tag{5}$$

Where, i_{Ls1} is the current of L_{s1}. u_{b1} and u_{b2} represent the voltage of the branch circuit of the primary and receiving sides, respectively. u_{ps1} and u_{ps2} represent the voltage of the signal detection resistor on the primary and receiving sides, respectively. u_{RL} is the voltage of the load R_L. G_{adi}(i=1,…,6) represent the transfer functions of the intermediate variables i_{Ls1}, u_{b1}, u_{b2}, u_{ps1}, and u_{ps2} which are adopted to simplify the solving process and the solution. Based on Equation (4) and Equation (5), the three transfer functions can be obtained as:

$$\begin{cases} G_{ps1} = \dfrac{u_{ps1}}{u_p} = G_{ad1}G_{ad2}G_{ad5} \\ G_{ps2} = \dfrac{u_{ps2}}{u_p} = G_{ad1}G_{ad2}G_{ad3}G_{ad5} \\ G_{RL} = \dfrac{u_{RL}}{u_p} = G_{ad1}G_{ad2}G_{ad3}G_{ad6} \end{cases} \tag{6}$$

G_{ps1} and G_{ps2} are the transfer functions from the power input voltage u_p to the signal detection resistor voltages u_{ps1} and u_{ps2}, which are adopted to measure the power interference with the signal transmission. G_{RL} is the transfer function from the power input voltage u_p to the load voltage u_{RL} after the addition of the communication branch circuit. Comparing G_{RL} in Equation (6) to G_{RL} in Equation (3), the impact of the additional communication branch circuit on the power transmission can be measured.

B. Signal Transmission

For power transfer, the inductors and capacitors of the resonance tank in Fig.3 should satisfy Equation (7).

$$\begin{cases} \omega_p^2 L_p C_p - 1 = 0 \\ \dfrac{\omega_p^2 C_{s1} C_{s2} \left(L_{s1} + L_{s2}\right)}{C_{s1} + C_{s2}} - 1 = 0 \end{cases} \tag{7}$$

Where ω_p is resonance angular frequency of the power resonance tank, where the parameters L_p, C_p, C_{s1}, C_{s2}, L_{s1}, and L_{s2} are marked in Fig. 3. Generally, the signal frequency ω_s is

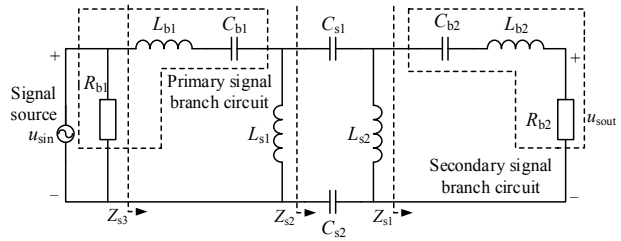

Fig. 5. Simplified circuit of signal channel.

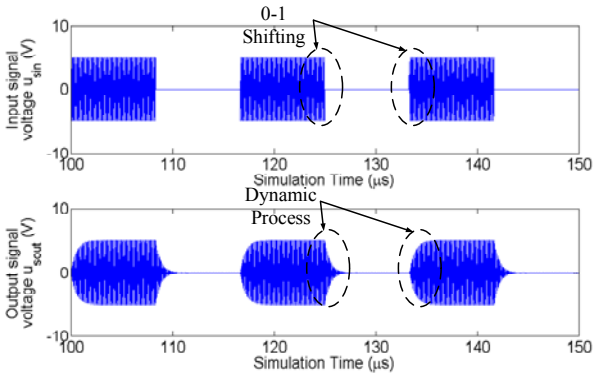

Fig. 6. The input signal waveform and output signal waveform.

much higher than the power wave frequency ω_p which is defined in Equation (8).

$$\omega_s = \alpha\omega_p \quad (\alpha \gg 1) \tag{8}$$

Where α is the ratio of the signal and power wave frequencies. Define the impedance on the left side of the primary signal branch and the right side of the secondary signal branch as Z_{left} and Z_{right}, respectively. They can be obtained as follows:

$$\begin{aligned} Z_{left} &= j\omega_s L_{s1} + \frac{j\omega_s L_p}{1-\omega_s^2 L_p C_p} \\ &= j\omega_s L_{s1} + \frac{\alpha}{j\omega_p C_p\left(\alpha^2-1\right)} \end{aligned} \tag{9}$$

$$Z_{right} = j\omega_s L_{s2} + R_L \tag{10}$$

In Equation (9), $\alpha/(\alpha^2-1)$ is approximately equal to $1/\alpha$ since α is much bigger than 1 which means that $j\omega_s L_p$ is much bigger than $1/j\alpha\omega_p C_p$. Therefore, the second term can be ignored. Similarly, for Equation (10), $j\omega_s L_{s2}$ is much bigger than R_L. Therefore, R_L can also be neglected. As a result, Equation (9) and Equation (10) can be approximately simplified as:

$$\begin{cases} Z_{left} = j\omega_s L_{s1} \\ Z_{right} = j\omega_s L_{s2} \end{cases} \tag{11}$$

Since L_{s1} is equal to L_{s2}, the analysis of the communications in both directions are the same due to above analyses. Therefore, for the communication signal channel, both the signal transmission from the transmitting side to the receiving side and the transmission from the receiving side to the transmitting side in Fig. 3 can be simplified as Fig. 5.

The attenuation coefficient of the signal channel is the transfer function from the signal source voltage u_{sin} to the voltage of the signal detection resistor u_{sout} without power transmission. The circuit in Fig. 5 is divided into four parts with certain impedances which are shown in Equation (12).

$$\begin{cases} Z_{s1} = \dfrac{1}{j\omega_s C_{b2}} + j\omega_s L_{b2} + R_{b2} \\ Z_{s2} = \dfrac{1}{j\omega_s C_s} + \dfrac{j\omega_s L_{s2} Z_{s1}}{j\omega_s L_{s2} + Z_{s1}} \\ Z_{s3} = \dfrac{1}{j\omega_s C_{b1}} + j\omega_s L_{b1} + \dfrac{j\omega_s L_{s1} Z_{s2}}{j\omega_s L_{s1} + Z_{s2}} \end{cases} \tag{12}$$

Where Z_{s1}, Z_{s2}, and Z_{s3} are shown in the Fig.5. L_b=L_{b1}=L_{b2}, C_b=C_{b1}=C_{b2}, R_b=R_{b1}=R_{b2}, and C_s=$C_{s1}C_{s2}/(C_{s1}$+$C_{s2})$. According to the Kirchhoff voltage and current laws (KVL and KCL), the intermediate transfer functions can be expressed as:

$$\begin{cases} G_{s1} = \dfrac{i_{Lb1}}{u_{sin}} = \dfrac{1}{Z_{s3}} \\ G_{s2} = \dfrac{i_{Cs1}}{i_{Lb1}} = \dfrac{Z_{s3} - j\omega_s L_{b1} - 1/j\omega_s C_{b1}}{Z_{s2}} \\ G_{s3} = \dfrac{i_{Lb2}}{i_{Cs1}} = \dfrac{Z_{s2} - 1/j\omega_s C_s}{Z_{s1}} \\ G_{s4} = \dfrac{u_{sout}}{i_{Lb2}} = R_{b2} \end{cases} \tag{13}$$

Where i_{Ls1}, i_{Cs1}, and i_{Lb2} are the currents of L_{s1}, C_{s1} and L_{b2}, respectively. u_{Rb2} represents the voltage of the signal detection resistor. $G_{si}(i$=1,…,4) represents the transfer functions of the intermediate variables i_{Lb1}, i_{Cs1}, and i_{Lb2}. Based on the Equation (12) and Equation (13), the transfer function from the signal source voltage u_{sin} to the voltage of the signal detection resistor u_{sout} can be obtained as:

$$G_s = \frac{u_{sout}}{u_{sin}} = G_{s1}G_{s2}G_{s3}G_{s4} \tag{14}$$

The transfer function G_s can be used to measure the attenuation coefficient of the signal channel.

IV. Dynamic Analysis of the Signal Transmission

A dynamic analysis is used to study the saltus step of the amplitude of the carrier wave while 0-1 shifting. After the amplitude of the carrier wave shifts between 0 and 1, the voltage on the detection resistor R_{b2} will reach the steady state after a start-up or a decay process (in Fig. 6). The duration of this start-up or decay process is related to the value of the parameters on the communication branch circuit.

In Fig. 5, the impedances of the inductors L_{s1} and L_{s2} can be simplified as an open circuit due to being extremely large under a high-frequency signal excitation. The coupling capacitors C_{s1} and C_{s2} can be neglected since their values are

relative large compared to C_{b1} and C_{b2}. Therefore, Fig. 5 can be simplified as Fig. 7.

Where L_e=L_{b1}+L_{b2}, and C_e=$C_{b1}C_{b2}$/(C_{b1}+C_{b2}). When the amplitude of the signal carrier wave shifts, a freely damped oscillation occurs in the communication signal channel. During the damped oscillation, the differential equation in terms of the voltage across the equivalent capacitor C_e and the detection resistor R_{b2} can be obtained as:

$$\begin{cases} \dfrac{\mathrm{d}^2 u_{ce}(t)}{\mathrm{d}t^2} + \dfrac{R_{b2}}{L_e}\dfrac{\mathrm{d}u_{ce}(t)}{\mathrm{d}t} + \dfrac{1}{L_e C_e}u_{ce}(t) = 0 \\ u_{ce}\big|_{t=0} = 0\,;\, du_{ce}/dt\big|_{t=0} = u_1/R_{b2}C_e \\ u_{Rb2} = R_{b2}C_e\dfrac{\mathrm{d}u_{ce}}{\mathrm{d}t} \end{cases} \tag{15}$$

The voltage of the resistor R_{b2} can be derived as:

$$u_{sout}(t) = \hat{u}_{sin} e^{-\frac{R_{b2}}{2L_e}t}\cos\omega_s t \tag{16}$$

Where, $\hat{u}_{sin}$ is the peak value of u_{sin} when the modulating signal is 1. The detailed derivation process of Equation (16) is provided in the Appendix. The function curve of the expression in Equation (16) is shown in Fig. 8.

To measure and define the duration of the dynamic process, the variable τ, which is the time when the amplitude of u_{sout} drops to $0.3\hat{u}_{sin}$, is introduced. The coefficient 0.3 is determined according to the reference voltage of the comparator in the demodulation step. Since the duration of the dynamic process affects the precision of the demodulation and results in a delay in the communication, the duration τ should be limited to within a defined range. In this paper, the duration τ is defined as $\tau = 15\%T_m/2$, where T_m is the modulation period. Based on Equation (16) and the definition of the variable τ, an new equation can be obtained as below.

$$-\frac{0.15R_{b2}T_m}{4L_e} = \ln 0.3 \tag{17}$$

Based on Equation (1) and Equation (17), the relationship between R_b and C_b can be derived as:

$$R_{b2}C_b = \frac{8\ln 0.3}{-0.15\omega_s^2 T_m} \tag{18}$$

Then the value of the isolation capacitor C_b is the only variable on the communication branch circuit. Both the values of the resistor R_b and the inductor L_b can be calculated according to C_b. Based on the dynamic analysis, the system parameters are chosen, and are shown in Table I.

Fig. 9 shows the values of the transfer functions G_{ps1}, G_{ps2}, G_{RL}, and G_s whose independent variable is C_b. In Fig.9, the According to Fig.9 (1) and Fig.9 (2), with an increase of C_b, the values of G_{ps1} and G_{ps2} decrease a little but the decreasing value range of the isolation capacitor C_b is from 1pF to 50pF.

amplitude is small. Therefore, the effect of the isolation capacitor C_b on the values of G_{ps1} and G_{ps2} can be ignored. However, in Fig.9 (3), the function G_{RL} decreases from 100% to 83% while the value of C_b increases. In Fig. 9 (4), the function G_s also decreases from 100% to 84% while the value of C_b increases. In conclusion, the power interference is kept constant while C_b increases. However, the power and signal attenuate significantly while C_b is set to a large value. To make a tradeoff, the isolation capacitor C_b is set to a small value 4.7pF which is the minimum value of a common silvered mica capacitor. Then the inductor L_b is derived as 53.9μH and R_b is 207.6Ω. All of the values of the elements in the communication branch circuit are listed in Table II.

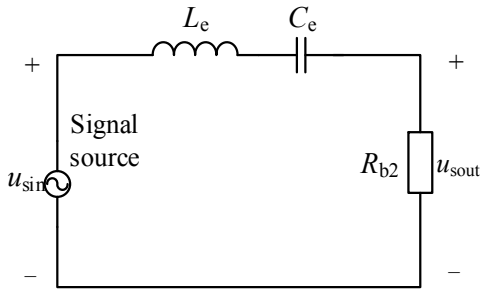

Fig. 7. Equivalent circuit model of signal channel dynamic characteristic.

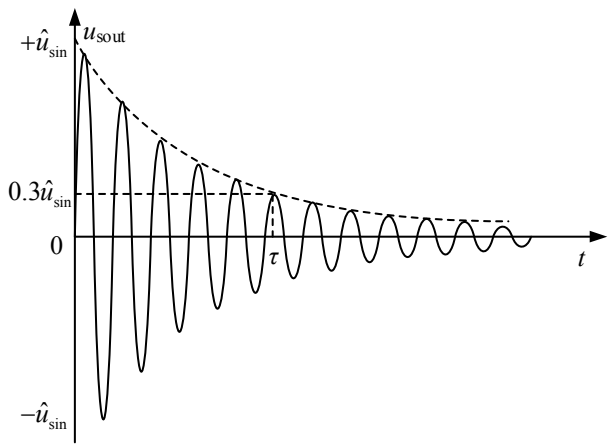

Fig. 8. Curves of signal carrier wave in dynamic procedure.

TABLE I
COMPONENTS PARAMETERS OF PUSH-PULL RESONANT ECPT SYSTEM

Parameters	Values
Input dc voltage E_{dc} (V)	15
Phase-splitting transformer L_{dc1}, L_{dc2} (mH)	1
Parallel resonant inductor L_p (μH)	11.8
Parallel resonant capacitor C_p (nF)	10
Series resonant inductor L_{s1}, L_{s2} (μH)	47.1
Coupling capacitor C_{s1}, C_{s2} (nF)	2.5
Resistor load R_L (Ω)	10
Angular frequency of power wave (kHz)	464
Angular frequency of signal wave (MHz)	10

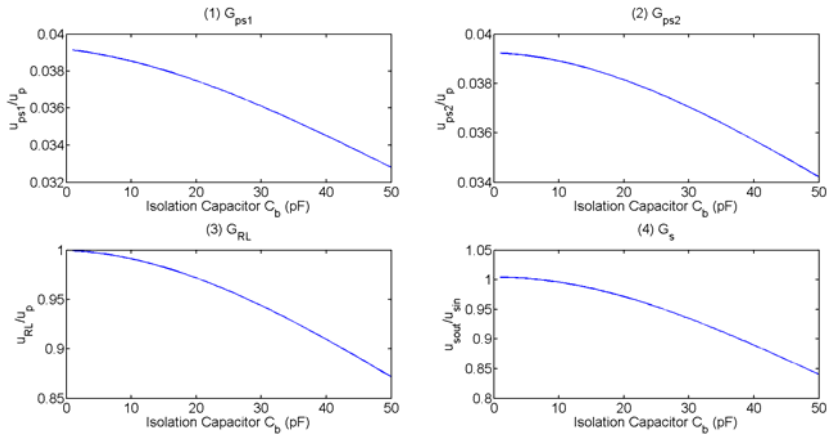

Fig. 9. The relationship between the values of transfer functions G_{ps1}, G_{ps2}, G_{RL}, G_s and isolation capacitor.

TABLE II
COMPONENTS PARAMETERS OF COMMUNICATION BRANCH CIRCUIT

Parameters	Values
Isolation capacitor C_b (pF)	4.7
Compensation inductor L_b (μH)	53.9
Signal detection resistor R_b (Ω)	207.6

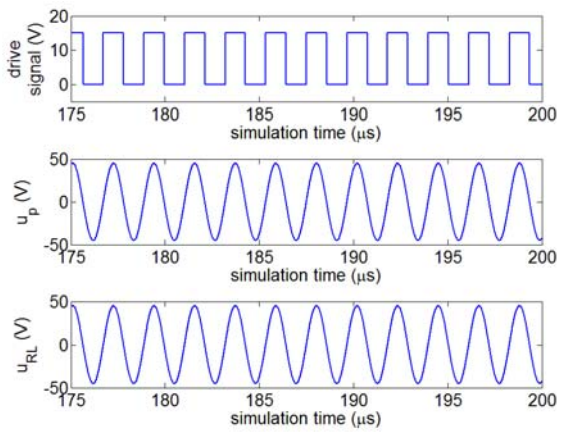

(a) Simulation waveforms of traditional ECPT system without communication branch circuits.

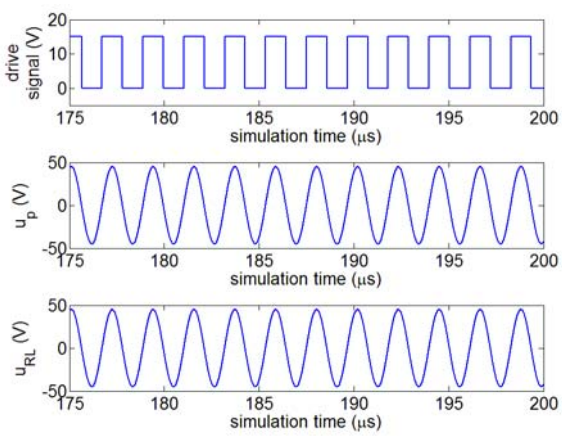

(b) Simulation waveforms of traditional ECPT system with communication module.

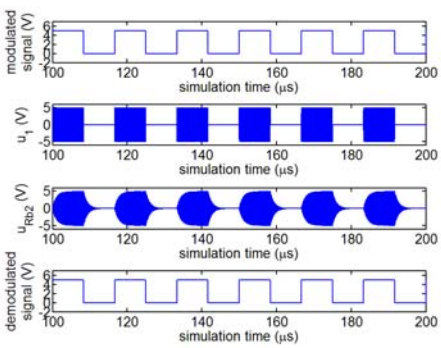

(c) Simulation waveforms of signal transmission without power interference.

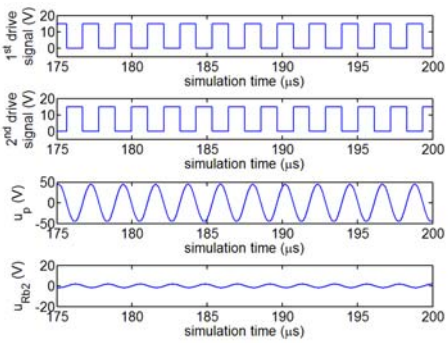

(d) Simulation waveforms of power interference on the signal detection resistor without signal transmission.

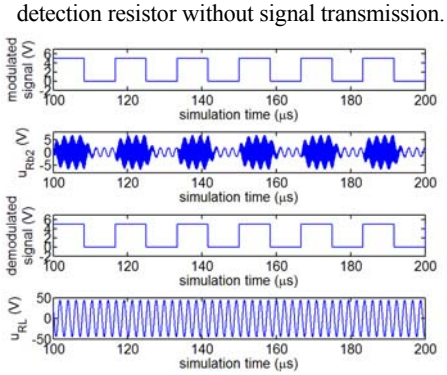

(e) Simulation waveforms power and signal transfer synchronously.

Fig. 10. Simulation waveforms of ECPT system with communication module.

V. Simulation Verification

The topology which is shown in Fig. 3 has been simulated using MATLAB Simulink. The input dc voltage of the power is set to 15V, and the component parameters on the main circuit are presented in Table I and Table II. The total simulation time was 100μs for the signals and 25μs for the power. In addition, the maximum simulation step was 1ns. The carrier frequency of u_1 was 10.0MHz. The amplitude of u_1 was 5V. The signal modulation frequency of u_1 was 60 kHz.

In Fig. 10(a), the drive signal and voltage of a traditional ECPT system without communication branch circuits are shown. The first waveform is the driving signal of the MOSFET. The second waveform is the voltage of the parallel resonant tank with an amplitude of 45.5V. The third waveform is the voltage across the load with an amplitude of 45.5V. The output power is 103.5W.

Fig. 10(b) presents waveforms of an ECPT system with a communication module. All three of the waveforms are extremely close to those in Fig. 8(a). This indicates that the communication branch circuit has little impact on wireless power transfer.

In Fig. 10(c), waveforms of signal transmission without wireless power transferring are shown. The first waveform is the modulated signal of the transmitting side whose modulation frequency is 60 kHz. The second waveform is the input signal u_1 with an amplitude of 5V. The third waveform is the voltage of the signal detection resistor R_{b2} with an amplitude of 5V. The last waveform is the demodulation signal whose demodulation frequency is 60 kHz which equalizes a data rate of 120 kbps.

Fig. 10(d) shows the power interference on the communication branch circuits when there is wireless power transferring without signal transmission. The first two waveforms are the driving signal of the MOSFETs. The third waveform is the voltage on the parallel resonant tank with an amplitude of 45.5V. The last waveform is the voltage on the signal detection resistor R_{b2} which is excited by u_p. Since the amplitude of the voltage on the signal detection resistor R_{b2} is 1.9V, the impact from the power transferring on the signal transfer is acceptable.

In Fig. 10(e), the waveforms of signal transmission with synchronous power transferring are shown. The first waveform is the modulated signal. The second waveform is the voltage of the signal detection resistor R_{b2}. The third waveform is the demodulation signal. The last waveform is the voltage on the load R_L. Based on the amplitude of the load voltage, which is 45V, the output power is calculated to be 101.3W.

VI. Experimental Verification

A. Experimental Setup

A practical ECPT experimental setup, with the parameters shown in Table I and Table II, has been built and tested.

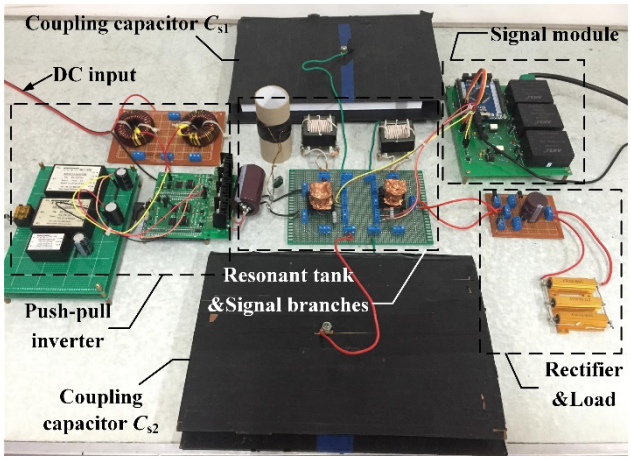

Fig.11 The experimental setup of the proposed ECPT system.

The experimental setup of the proposed ECPT system is presented in Fig. 11. There are four parts: 1) the push-pull inverter; 2) the power resonant tank and signal branches; 3) the rectifier and load; 4) the signal module.

B. Experimental Waveforms and Discussion

All of the waveforms in Section IV are tested on the experimental setup and the experimental waveforms are shown in Fig. 12.

Comparing Fig.12 (a) with Fig. 12(b), it can be seen that the branch circuits have a small impact on wireless power transfer since there is a negligible change in the amplitudes of the output voltages. The power efficiencies test results of a traditional ECPT system with or without branch circuits are both higher than 85%. In Fig. 12(c) the signal attenuation is small, which indicates that the signal can be transmitted through the system without changes or errors. Fig. 12(d) verifies that power flow has a small impact on the signal transmission since the amplitude of the voltage at the channel terminals is approximately 2.5 times smaller than the amplitude of the signals. Fig. 12(e) shows that the power and signal can be transferred synchronously in the sharing channel due to the slight signal amplitude change and the high amplitude of the load voltage.

Comparing Fig. 10 with Fig. 12, it can be seen that the simulation waveforms are slightly different from the experimental waveforms since the ultra-high frequency of the carrier wave increase the internal resistance of the inductors L_{b1} and L_{b2}. Therefore, the amplitude of the voltage on the detection resistor in Fig. 12(c) is slightly lower than the simulation results in Fig. 10(c).

Moreover, the resonant voltage and the pick-up voltage on the load are both slightly lower than the simulation voltage. This is due to the fact that the stray parameters of the components in the circuit, such as the internal resistance, were not considered in the simulations. However, all of these differences have insignificant impacts on the system and can be ignored. This makes the experimental results match the simulations. In

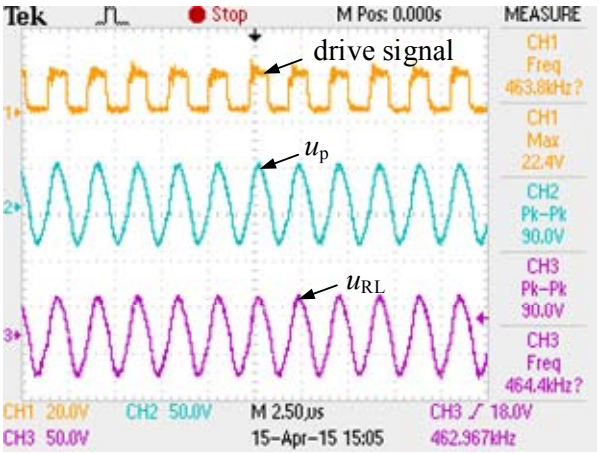

(a) Experiment waveforms of traditional ECPT system without communication branch circuits.

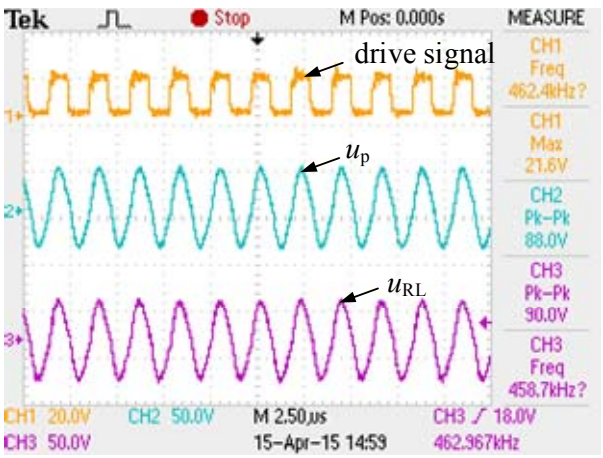

(b) Experiment waveforms of traditional ECPT system with communication module.

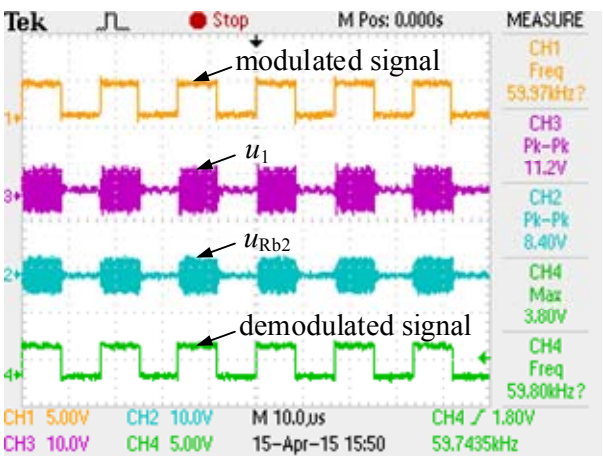

(c) Experiment waveforms of signal transmission without power interference.

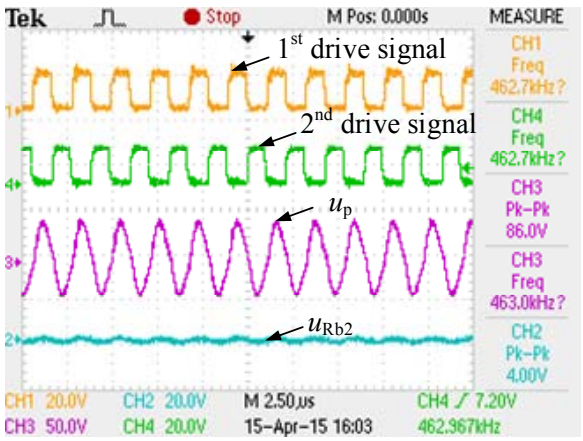

(d) Experiment waveforms of power interference on the signal detection resistor without signal transmission.

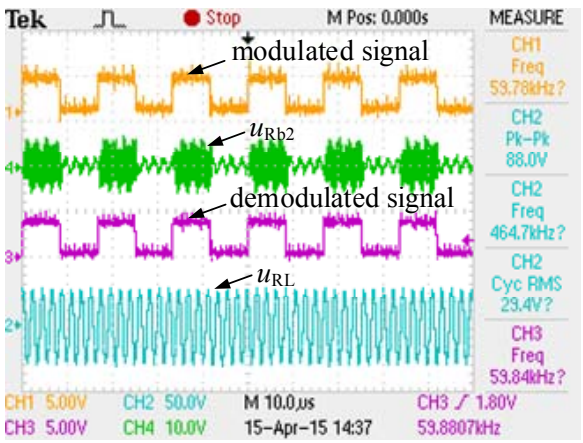

(e) Experiment waveforms power and signal transfer synchronously.

Fig.12. Experiment waveforms of ECPT system with communication module.

conclusion, both the simulation results and the experimental results verify the correctness and effectiveness of the proposed wireless power and signal transfer method.

In this paper, the application object is an ECPT system whose control signal or detection signal is transmitting and receiving by the microcontroller units (MCU). Generally, MCU of ECPT systems communicate with external devices by serial communication. The standard data rates of serial communications are specific values in the range of 300 bps-115.2 kbps, such as 9600 bps, 19200 bps, and 115200 bps. In this study, over 100W of power and signal with a data rate from 300bps to 120 kbps can be well transferred without data losses. This is sufficient for the data rate of the common serial communication in engineering applications.

C. Further Discussion

All of the work presented in this paper focus on the topology and characteristics of a system and method to transfer power and a signal in a shared channel. If a higher data rate is needed in some applications, the data rate limitation of the proposed system and its influencing factors make it important to measure the capacity of a communication system. Therefore, a study on the data rate limitation is meaningful for further research.

VII. Conclusion

Based on the traditional ECPT topology for wireless power transfer, a power and signal shared channel was proposed. The operating principle of the designed channel was explained, and the electrical circuit components of the proposed channel were calculated based on an analysis of the mutual interference between the power and signal channel; the power and signal attenuation; and the dynamic characteristic of the signal channel. Both simulations and experimental results verified the correctness and effectiveness of the proposed wireless power and signal transfer method. Finally, the designed channel can simultaneously transfer over 100W of output power and data with a data rate from 300bps to 120 kbps.

Appendix

For the differential equation, Equation (16) in terms of the voltage across the equivalent capacitor C_e. The voltage of the capacitor C_e can be obtained as:

$$u_{ce}(t) = e^{-\alpha t}\frac{u_1}{\beta R_{b2} C_e}\sin\beta t$$

Where α is the damping coefficient, and β is the operating frequency in the free resonant mode, which can be given by:

$$\alpha = \frac{R_{b2}}{2L_e},\ \beta = \sqrt{\frac{1}{L_e C_e} - \frac{R_{b2}^2}{4L_e^2}}$$

Because $1/L_e C_e \gg R_{b2}^2/4L_e^2$, $\beta \approx 1/\sqrt{L_e C_e} = \omega_s$. Therefore, the voltage of the capacitor C_e can be expressed as:

$$u_{ce}(t) = e^{-\frac{R_{b2}}{2L_e}t}\frac{u_1}{\omega_s R_{b2} C_e}\sin\omega_s t$$

Then the voltage of the detection resistor R_{b2} can be obtained as:

$$\begin{aligned} u_{Rb2} &= R_{b2} i_{ce} = R_{b2} C_e \frac{\mathrm{d}u_{ce}}{\mathrm{d}t} \\ &= \frac{u_1}{\omega_s} e^{-\frac{R_{b2}}{2L_e}t}\left(\omega_s \cos\omega_s t - \frac{R_{b2}}{2L_e}\sin\omega_s t\right) \end{aligned}$$

Because $\omega_s \gg R_{b2}/2L_e$, the voltage of the detection resistor R_{b2} can be simplified as:

$$u_{Rb2} = u_1 e^{-\frac{R_{b2}}{2L_e}t}\cos\omega_s t$$

Acknowledgment

This work was sponsored by the research funds for the National Natural Science Foundation of China under Grants #51477020 and #51277192. This work was also supported by Chongqing International Science and Technology Cooperation Base Project under Grants CSTC2015GJHZ40001.

References

[1] A. Kurs, A. Karalis, R. Moffatt, J. D. Joannopoulos, P. Fisher, and M. Soljacic, "Wireless power transfer via strongly coupled magnetic resonances," *Science Magazine*, Vol. 317, pp. 83-86, Jul. 2007.

[2] G. A. Covic and J. T. Boys, "Inductive power transfer," *Proceedings of the IEEE*, Vol. 101, No. 6, pp. 1276-1289, Jun. 2013.

[3] D. C. Ludois, M. J. Erickson, and J. K. Reed, "Aerodynamic fluid bearings for translational and rotating capacitors in noncontact capacitive power transfer systems," *IEEE Trans. Ind. Appl.*, Vol. 50, No. 2, pp. 1025-1033, Mar./Apr. 2014.

[4] A. P. Hu, L. Chao, and L. L. Hao, "A novel contactless battery charging system for soccer playing robot," in *15th International Conference on Mechatronics and Machine Vision in Practice(M2VIP)*, pp. 646-650, Dec. 2008.

[5] A. I. Al-Kalbani, M. R. Yuce, and J. M. Redoute, "A biosafety comparison between capacitive and inductive coupling in biomedical implants," *IEEE Antennas Wireless Propag. Lett.*, Vol. 13, pp. 1168-1171, Jun. 2014.

[6] L. Chao, A. P. Hu, B. Wang, and N. C. Nair, "A capacitively coupled contactless matrix charging platform with soft switched transformer control," *IEEE Trans. Ind. Electron.*, Vol. 60, No. 1, pp. 249-260, Jan. 2013.

[7] J. Kim and F. Bien, "Electric field coupling technique of wireless power transfer for electric vehicles," in *IEEE TENCON Spring Conference*, pp. 267-271, Apr. 2013.

[8] J. Dai and D. C. Ludois, "Wireless electric vehicle charging via capacitive power transfer through a conformal bumper," in *IEEE Applied Power Electronics Conference and Exposition(APEC)*, pp. 3307-3313, Mar. 2015.

[9] C. Liu, A. P. Hu, and N. K. C. Nair, "Modelling and analysis of a capacitively coupled contactless power transfer system," *IET Power Electronics,* Vol. 4, No. 7, pp. 808-815, Aug. 2011.

[10] M. P. Theodoridis, "Effective capacitive power transfer," *IEEE Trans. Power Electron.*, Vol. 27, No. 12, pp. 4906-4913, Dec. 2012.

[11] Y. Su, X. Dai, Z. Wang, C. Tang, and Y. Sun, "Study on an optimal control method for energy injection resonant AC/AC high frequency converters," *Journal of Power Electronics*, Vol. 13, No. 2, pp. 197-205, Mar. 2013.

[12] A. Abdolkhani and A. P. Hu, "Improved autonomous current-fed push-pull resonant inverter," *IET Power Electronics,* Vol. 7, No. 8, pp. 2103-2110, Aug. 2014.

[13] X. Dai, Y. Zou, and Y. Sun, "Uncertainty modeling and robust control for LCL resonant inductive power transfer system," *Journal of Power Electronics*, Vol. 13, No. 5, pp. 814-828, Sep. 2013.

[14] C. Tang, Y. Sun, X. Dai, Y. Su, S. K. Nguang, and A. P. Hu, "Shifting stable operating points of bifurcated IPT systems by time delay perturbation," *Electronics Letters*, Vol. 49, No. 9, pp. 615-617, Apr. 2013.

[15] H. L. Li, A. P. Hu, and G. A. Covic, "Primary current generation for a contact less power transfer system using free oscillation and energy injection control," *Journal of Power Electronics*, Vol. 11, No. 3, pp. 256-263, May 2011.
[16] G. Wang, P. Wang, Y. Tang, and W. Liu, "Analysis of dual band power and data telemetry for biomedical implants," *IEEE Trans. Biomed. Circuits Syst.*, Vol. 6, No. 3, pp. 208-215, Jun. 2012.
[17] A. D. Rush and P. R. Troyk, "A power and data link for a wireless-implanted neural recording system," *IEEE Trans. Biomed. Eng.*, Vol. 59, No. 11, pp. 3255-3262, Nov. 2012.
[18] S. Mandal and R. Sarpeshkar, "Power-efficient impedance-modulation wireless data links for biomedical implants," *IEEE Trans. Biomed. Circuits Syst.* Vol. 2, No. 4, pp. 301-315, Dec. 2008.
[19] G. Yilmaz, O. Atasoy, and C. Dehollain, "Wireless energy and data transfer for in-vivo epileptic focus localization," *IEEE Sensors J.*, Vol. 13, No. 11, pp. 4172-4179, Nov. 2013.
[20] J. Hirai, T.-W. Kim, and A. Kawamura, "Integral motor with driver and wireless transmission of power and information for autonomous subspindle drive," *IEEE Trans. Power Electron.*, Vol. 15, No. 1, pp. 13-20, Jan. 2000.

Yu-Gang Su received his B.S. and M.S. degrees in Industry Automation, and his Ph.D. degree in Control Theory and Control Engineering from Chongqing University, Chongqing, China, in 1985, 1993, and 2004, respectively. From 2008 to 2009, he was a visiting scholar at the University of Queensland, Brisbane, Australia. He is presently working as a Professor in the College of Automation, Chongqing University. His current research interests include power electronics, control theory and applications, and wireless power transfer.

Wei Zhou received his B.S. degree from the College of Automation, Chongqing University, Chongqing, China, in 2013, where he is presently working towards his Ph.D. degree in Control Theory and Control Engineering. His current research interests include capacitively coupled power transfer technologies, parallel wireless power and signal transmission, and control theory.

Aiguo Patrick Hu received his B.S. and M.S. degrees from Xi'an JiaoTong University, Xi'an, China, in 1985 and 1988, respectively. He received his Ph.D degree from the University of Auckland, Auckland, New Zealand, in 2001. He then served as a Lecturer and as a Director of the China Italy Cooperative Technical Training Center, Xi'an, China. He also served as the General Manager of a technical development company. He spent a smemster as an exchange postdoc research fellow at the National University of Singapore (NUS), Singapore, with funding from the Asian2000 Foundation. He holds 15 patents in wireless/contactless power transfer and microcomputer control technologies. He has published more than 200 peer reviewed journal and conference papers, authored a monograph on wireless inductive power transfer technology, and contributed 4 chapters to a book. Dr Hu is presently with the Department of Electrical and Computer Engineering, University of Auckland. He is also the Head of Research at PowerbyProxi Ltd., Auckland, New Zealand. His current research interests include wireless/contactless power transfer systems, and the application of power electronics in renewable energy systems.

Chun-Sen Tang received his B.S. and Ph.D degrees from the College of Automation, Chongqing University, Chongqing, China, in 2004 and 2009, respectively. In 2008, he was a Research Fellow in the Department of Electrical and Computer Engineering, University of Auckland, Auckland, New Zealand. He joined College of Automation, Chongqing University, Chongqing, China, in 2009, and is prestntly an Associate Professor. His current research interests include nonlinear modeling and analysis, intelligent control, and wireless power transfer.

Rong Hua received his B.S. degree (Hons.) from the Department of Electrical and Computer Engineeing, University of Auckland, Auckland, New Zealand, in 2013, where he is presently working towards his Ph.D. degree. His current research interests include electromagnetic field modelling and wireless power transfer.